Fast ¹⁹F Magic Angle Spinning NMR for Structural Characterization of Active Pharmaceutical Ingredients in Blockbuster Drugs

Caitlin M. Quinn¹, Roman Zadorozhnyi^{1,2}, Jochem Struppe⁴, Ivan V. Sergeyev⁴, Angela M. Gronenborn^{2,3*}, Tatyana Polenova^{1,2*}

¹Department of Chemistry and Biochemistry, University of Delaware, Newark, Delaware 19716, United States; ²Pittsburgh Center for HIV Protein Interactions, University of Pittsburgh School of Medicine, 1051 Biomedical Science Tower 3, 3501 Fifth Avenue, Pittsburgh, PA 15261, United States; ³Department of Structural Biology, University of Pittsburgh School of Medicine, 3501 Fifth Ave., Pittsburgh, PA 15261, United States; ⁴Bruker Biospin Corporation, 15 Fortune Drive, Billerica, MA 01821, United States

*Corresponding authors: Tatyana Polenova, Department of Chemistry and Biochemistry, University of Delaware, Newark, DE, USA, Tel.: (302) 831-1968; Email: tpolenov@udel.edu; Angela M. Gronenborn, Department of Structural Biology, University of Pittsburgh School of Medicine, 3501 Fifth Ave., Pittsburgh, PA 15260, USA, Tel.: (412) 648-9959; Email: amg100@pitt.edu

Keywords: fast ¹⁹F MAS NMR, active pharmaceutical ingredients, API

ABSTRACT

Fluorinated drugs occupy a large and growing share of the pharmaceutical market. Here we explore high frequency, 60 to 111 kHz, magic angle spinning ¹⁹F NMR spectroscopy for structural characterization of fluorinated active pharmaceutical ingredients in commercial formulations of seven blockbuster drugs: Celebrex®, Cipro®, Crestor®, Levaquin®, Lipitor®, Prozac®, and Zyvox®. ¹⁹F signals can be observed in a single scan and spectra with high signal-to-noise can be acquired in minutes. ¹⁹F spectral parameters, such as chemical shifts and line widths are sensitive to both the nature of the fluorine moiety and the formulation. We anticipate that the fast MAS ¹⁹F NMR-based approach presented here will be valuable for rapid analysis of fluorine-containing drugs in a wide variety of formulations.

INTRODUCTION

Fluorine-containing molecules comprise 20-30% of all drugs in the pharmaceutical market, and their market share is constantly growing.¹⁻³ According to current estimates, fluorine atoms or fluoroalkyl groups are incorporated in over 150 commercial drugs, including some of the most-prescribed and/or most-profitable.¹⁻³ In 2019 alone, eleven new fluorine-containing drugs were approved by the FDA⁴. Indeed, fluorination has become an indispensable tool in the medicinal chemistry tool chest: introduction of fluorine into organic drug scaffolds allows for stalling metabolism, increasing lipophilicity, and fine-tuning pharmacokinetic properties.⁵ Diverse fluorine functionalities are employed, with monofluoro-, polyfluoro-, and trifluoromethyl substituents commonly incorporated into aromatic or aliphatic units.² In drug formulations, the active pharmaceutical ingredient (API) typically only comprises a fraction of the overall mixture. Therefore, characterization of drug formulations by NMR with commonly used ¹³C- or ¹H- detected experiments presents a challenge, since the spectrum invariably reports predominantly on the excipients⁶⁻⁹.

Fluorine or, specifically, the 100%-abundant magnetically active ¹⁹F isotope, is a powerful NMR beacon that has gained considerable attention as a unique probe in small-molecule pharmaceuticals and biological molecules. ¹⁰⁻²⁹ ¹⁹F, a spin-1/2 nucleus, possesses very high sensitivity, similar to ¹H (0.85 vs 1) and ¹⁹F chemical shifts are exquisitely sensitive to the local structural and electronic environment, spanning a range of over 300 ppm. ³⁰ Given the prevalence of fluorinated drugs and fluorine's advantageous spectroscopic properties, it is surprising that fluorine NMR has been underutilized for analyzing pharmaceutical formulations compared to ¹H and ¹³C: to date, there are very few reports of ¹⁹F-based structural characterization of APIs in drug formulations, ³¹⁻³⁵ and little systematic data have been published. ¹⁹F MAS NMR offers a sensitive and convenient probe to complement ¹H and ¹³C studies of pharmaceutical formulations. Particularly, with fast spinning capabilities becoming more routine, ¹⁹F-based experiments that may not have been practical or informative at slower MAS frequencies enable observation of APIs in commercial formulations. These approaches include ¹⁹F-¹⁹F, ¹H-¹⁹F, and ¹³C-¹⁹F correlation spectroscopy. Furthermore, the improved ¹⁹F resolution observed with fast MAS frequencies permits extraction of detailed structural features otherwise not accessible.

Herein, we explore fluorine as a direct and sensitive reporter on APIs' local structure in the complex chemical environment of pharmaceutical formulations. For this study, we selected seven blockbuster drugs (i.e., drugs that generate annual sales of \$1 billion or more): the anti-inflammatory Celebrex® (celecoxib), the antidepressant Prozac® (API: fluoxetine hydrochloride), the cholesterol-lowering statins Crestor® (API: rosuvastatin calcium) and Lipitor (API: atorvastatin calcium), and the antibiotics Cipro® (API: ciprofloxacin hydrocholoride), Levaquin® (API: levofloxacin), and Zyvox® (API: linezolid). Given that all drug formulations are unique and often proprietary, we only have

knowledge about the fraction of the API in the individual tablets, which varies widely from 6.5 % w/w in Crestor® to 79% in Levaquin® (Table S1).

Our study demonstrates that 1D and 2D ¹⁹F-detected NMR experiments at 60 to 111 kHz magic angle spinning (MAS) frequency provide a time-effective and sensitive means to probe the API structure. The data reveal that fluorine chemical shifts report on conformational homo/heterogeneity of the API and permit the detection of crystallographically inequivalent sites. Importantly, it was possible to exploit the high sensitivity of the fluorine nucleus for indirect detection of ¹³C resonances of the APIs, which may be inaccessible otherwise due to low natural abundance and/or strong background signals from the excipients.

MATERIALS AND METHODS

Chemicals

Pharmaceutical formulations of celecoxib (Celebrex®, 200 mg capsule manufactured by Viatris), fluoxetine hydrochloride (Prozac®, 20 mg capsule manufactured by Eli Lily), rosuvastatin calcium (three generic formulations, 10 and 20 mg tablets manufactured by Biocon, Tris Pharma, and Kanon Pharma), atorvastatin calcium (two different generic formulations, 10 and 40 mg tablets, manufactured by Teva and Apotex), ciprofloxacin hydrochloride (generic, 500 mg tablet manufactured by Pack Pharmaceuticals), levofloxacin (two generic formulations, 750 mg tablets manufactured by Zydus and Camber), and linezolid (generic, 600 mg tablet manufactured by Teva), were used. For NMR spectroscopy, the individual formulations were finely ground into powders and packed into 1.3 or 0.7 mm MAS rotors. Each 1.3 mm rotor contained 2.6-3.2 mg of material, of which 0.17-2.38 mg were the fluorine-containing API. Each 0.7 mm rotor contained less than 0.5 mg of total material.

MAS NMR spectroscopy

 19 F and 13 C-detected experiments were performed on a 11.7 T wide bore Bruker AVANCE III spectrometer outfitted with a 1.3 mm HFX MAS probe. The Larmor frequencies were 500.13 MHz for 1 H, 470.59 MHz for 19 F and 125.76 MHz for 13 C. All MAS NMR spectra were acquired at a MAS frequency of 60 kHz maintained within ±10 Hz by Bruker MAS III controller. The sample temperature was calibrated with KBr as an external temperature sensor, and was maintained at 28±0.3 °C by a Bruker variable temperature controller. 19 F and 13 C chemical shifts were referenced with respect to those of trifluoroacetic acid (100 μM solution in 25 mM sodium phosphate buffer, pH 6.5) as an external reference (0 ppm) and adamantane, respectively. Typical 90° pulse lengths were 2.35 μs for 1 H, 2.39 μs for 19 F and 2.89 μs for 13 C. 19 F and 1 H spin-lattice relaxation rates were measured using a standard inversion-recovery sequence 36 .

For ¹H-¹³C CPMAS experiments, ¹H-¹³C cross polarization was performed with a linear ramp; the ¹H and ¹³C radio frequency (RF) fields were 105 kHz and 45 kHz, respectively; the typical CP contact times were 1.5-2 ms; the ¹³C carrier frequency was set to 100 ppm. The spectra were collected with 2816 scans (ciprofloxacin, 4 hrs 41 min), 2048 scans (fluoxetine, 3 hrs 59 min), 1024 scans (celecoxib, 2 hrs 50 min), 2048 scans (rosuvastatin, 3 hrs 25 min), 3072 scans (atorvastatin, 5 hrs 59 min). 3072 scans (linezolid, 5 hrs 7 min), and 3072 scans (levofloxacin, 3 hrs 25 min).

¹³C-¹⁹F cross-polarization was performed with a linear amplitude ramp of 70-100% on ¹³C, with the center of the ramp Hartmann-Hahn matched to the first spinning sideband; the ¹³C carrier frequency was set to 100 ppm. The ¹⁹F RF field was 15 or 35 kHz; the ¹³C RF field was 45 or 25 kHz. For ¹H-¹⁹F CPMAS experiments, ¹H-¹⁹F cross polarization was performed with a linear ramp; the ¹H and ¹⁹F RF fields were 105 kHz and 45 kHz, respectively; the typical CP contact time was 2 ms. For the 2D ¹H-¹⁹F HETCOR of levofloxacin a 0.5 ms contact time was used and 32 scans with 64 complex

points were acquired in the t_1 dimension. For atorvastatin, a 1.5 ms mixing was used, and 384 and 88 scans with 64 complex points were acquired with for generic formulations 1 and 2, respectively. 2D (1 H)- 13 C- 19 F HETCOR experiments on ciprofloxacin, fluoxetine, and levofloxacin, were acquired with 48, 144, and 144 scans, respectively; the 1 H- 13 C contact times were 1.5-2 ms; 13 C- 19 F CP contact times were 11, 7, and 10 ms; 64, 74, and 192 complex points, respectively, were acquired in the t_1 dimension. The carrier frequency in 13 C was set to 100.0 ppm. In several experiments, 19 F decoupling was performed with a rotor-synchronized π -pulse (RF field of 105 kHz), applied every second rotor period during evolution in the 13 C dimension. In most 19 F detected experiments, 15 kHz time-proportional phase modulation (TPPM) 37 1 H decoupling was applied during acquisition. Other acquisition parameters were sample-dependent and are provided in the corresponding figure legends. For chemical shift anisotropy (CSA) parameter determination of levofloxacin and atorvastatin, slow MAS spectra were acquired at 10 kHz MAS (Figure S2). The CSA values were determined with Herzfeld-Berger analysis (HBA) 38 and incorporated into delays alternating with nutation for tailored excitation - radio frequency driven recoupling (DANTE-RFDR) simulations described below.

The 1D ¹⁹F DANTE^{39,40} and DANTE-RFDR spectra of levofloxacin, atorvastatin calcium, and rosuvastatin calcium formulations were acquired with 32, 96, and 256 scans respectively. For frequency-dependent DANTE inversion experiments, 42-48 0.1-µs DANTE inversion pulses were applied on resonance for each peak in the spectra of levofloxacin and atorvastatin, and for rosuvastatin in 1 ppm steps between -22 and -43 ppm. The DANTE interpulse delays were set to 1 (levofloxacin peaks I-II), 2 (levofloxacin peaks III-IV) or 4 (atorvastatin, rosuvastatin) rotor cycles. For levofloxacin and atorvastatin, CP from ¹H was used for initial ¹⁹F excitation, to speed up data acquisition. The recycle delay was 4.0 s (levofloxacin), 6.0 s (atorvastatin) or 10 s (rosuvastatin). The (XY8)¹₄ or/and XY8 phase cycle⁴¹ was applied during the RFDR mixing. To account for zero-quantum (ZQ) relaxation occurring during RFDR mixing, control experiments were acquired without DANTE selective inversion. For levofloxacin, a series of 2D ¹⁹F-¹⁹F RFDR spectra were acquired with ¹H-¹⁹F CP, followed by a RFDR period; the mixing times were 10, 30, and 100 ms; 128 scans with 64 complex points were acquired in the t₁ dimension. For the atorvastatin ¹⁹F-¹⁹F RFDR spectrum, the mixing time was 20 ms, and 96 scans with 88 complex points were acquired in the t₁ dimension.

 19 F-detected experiments on atorvastatin were also performed at several MAS rotation rates between 60 and 111 kHz on a 11.7 T wide bore Bruker Neo spectrometer, outfitted with a 0.7 mm H/F-X MAS probe. The 19 F 90° pulse length was 1.0 μ s. The 2D 19 F- 19 F RFDR spectrum was acquired with 128 scans, the mixing time 100 ms, and 32 complex points in the t_1 dimension.

The 1D ¹³C CPMAS spectrum of Linezolid was acquired on a 14.1 T standard bore Bruker AVANCE III spectrometer outfitted with a 1.3 mm HCN MAS probe. The MAS frequency was 60 kHz

and was maintained within ±10 Hz by Bruker MAS III controller. The sample temperature was calibrated with KBr as an external temperature sensor and was maintained at 21±0.3 °C by a Bruker variable temperature controller. CP conditions and other experimental parameters were similar to those described above.

All spectra were processed in TopSpin 3.6 or 4.0 and analyzed in TopSpin or NMRFAM-Sparky⁴². All 1D ¹⁹F-detected spectra in Figures 1 and 2 (¹⁹F direct polarization and ¹H-¹⁹F CP) were processed with 10 Hz exponential apodization except spectra of rosuvastatin which were processed with 75 Hz exponential apodization. The 2D ¹⁹F-¹⁹F RFDR spectra of levofloxacin (Figure 3) and atorvastatin (Figure 4) were processed with 90° sinebell apodization in both dimensions. ¹⁹F-detected spectra of atorvastatin in Figure 4f were processed without apodization. (¹H)¹³C-¹⁹F 2D HETCOR spectra were processed as follows: ciprofloxacin (Figure 2e), 60° sinebell (t₂) and 128 points linear prediction followed by 75° sinebell apodization (t₁); fluoxetine (Figure 2f), 200 Hz (t₂) and 75 Hz (t₁) exponential apodization; levofloxacin (Figure 3f), 75° (t₂) and 90° (t₁) sinebell apodization. 2D ¹H-¹⁹F HETCOR spectra were processed as follows: levofloxacin (Figure 3g), 90° sinebell apodization in both dimensions; atorvastatin (Sample 1, Figure 4d), 32 points linear prediction in t₁ followed by 90° sinebell apodization in both dimensions; atorvastatin (Sample 2, Figure 4d) 75° sinebell apodization in both dimensions.

Numerical simulations

The DANTE-RFDR magnetization exchange curves were simulated in SIMPSON⁴³ (version 4.2.1). In the two-spin simulations, the magnetization originated on the non-selectively saturated spin, I_{2z} , followed by the magnetization exchange to $-I_{1z}$. An example simulation script is presented in the Supporting Information. The simulated curves were corrected for ZQ relaxation using the experimentally determined ZQ relaxation rates.

RESULTS

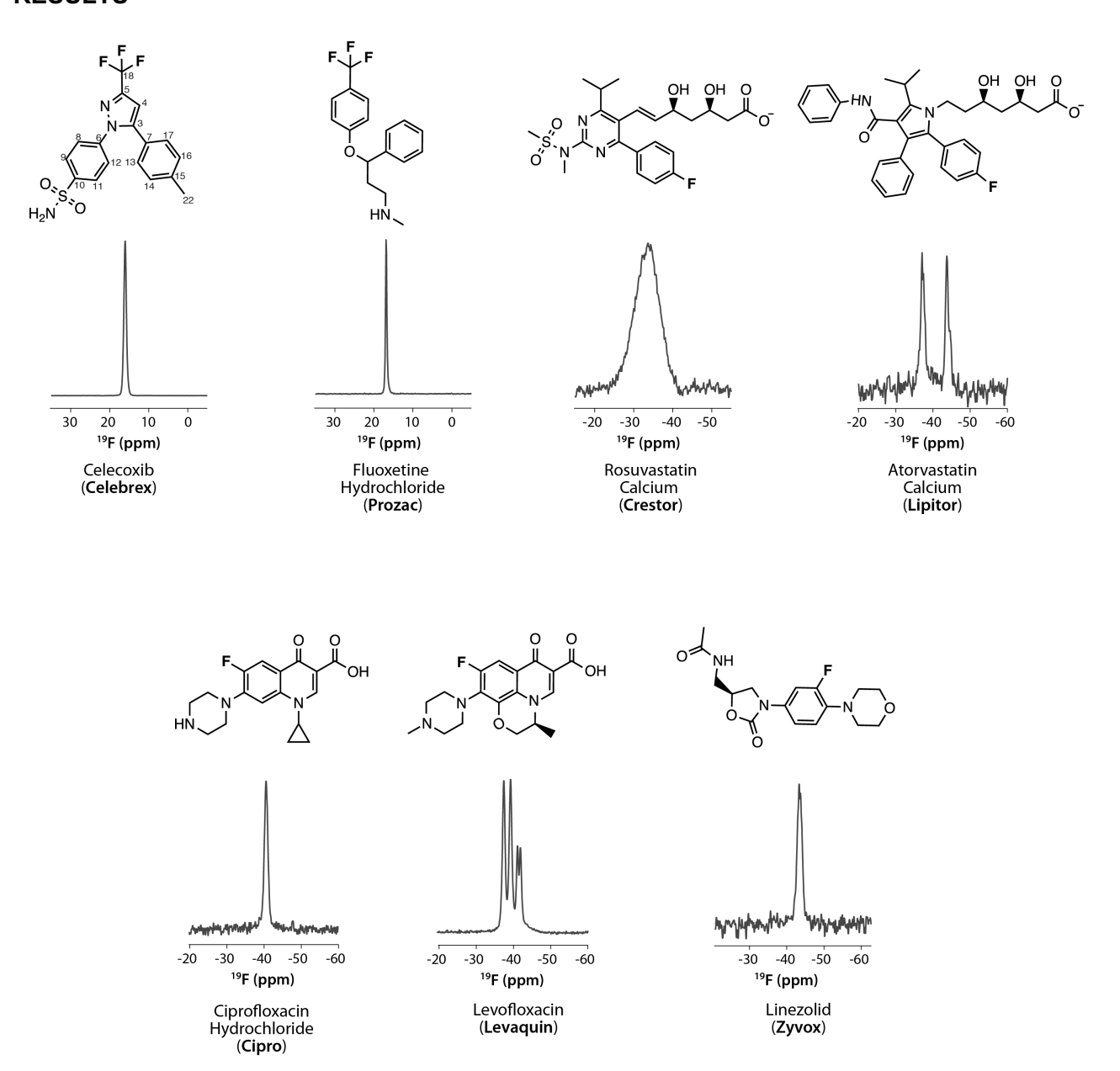


Figure 1. Chemical structures and ¹⁹F MAS spectra of APIs in drug formulations of celecoxib, fluoxetine hydrochloride, rosuvastatin calcium, atorvastatin calcium, ciprofloxacin hydrochloride, linezolid, and levofloxacin. The brand name of the drug is provided in parentheses. All spectra were acquired with 16 scans, except for that of rosuvastatin calcium, for which 128 scans were recorded. ¹H TPPM decoupling (15 kHz) was applied during acquisition. The total acquisition times were: 50 s (celecoxib), 2 min 40 s (ciprofloxacin), 75 min (rosuvastatin), 2 m 40 s (levofloxacin), 10 min 40 s (atorvastatin), 2 min 40 s (fluoxetine), and 13 min 20 s (linezolid). The MAS frequency was 60 kHz.

¹⁹F 60 kHz MAS NMR spectra for all seven pharmaceutical formulations (Figure 1), exhibited intense, relatively sharp resonances, except rosuvastatin calcium, for which a broad envelope was observed. Strong signals were obtained with a single scan and high-quality spectra were acquired in less than 2-3 minutes. For atorvastatin and linezolid, the spectra were recorded in 10-15 minutes due to longer ¹⁹F T₁s (Table S1). Acquiring the spectrum of generic formulations of rosuvastatin with

comparable signal-to-noise ratio (SNR) required more signal averaging due to the large, heterogeneous linewidth. When 19 F T_1 s exceeded 10 s, 1 H- 19 F cross polarization permitted faster spectral acquisition (Figure 2a).

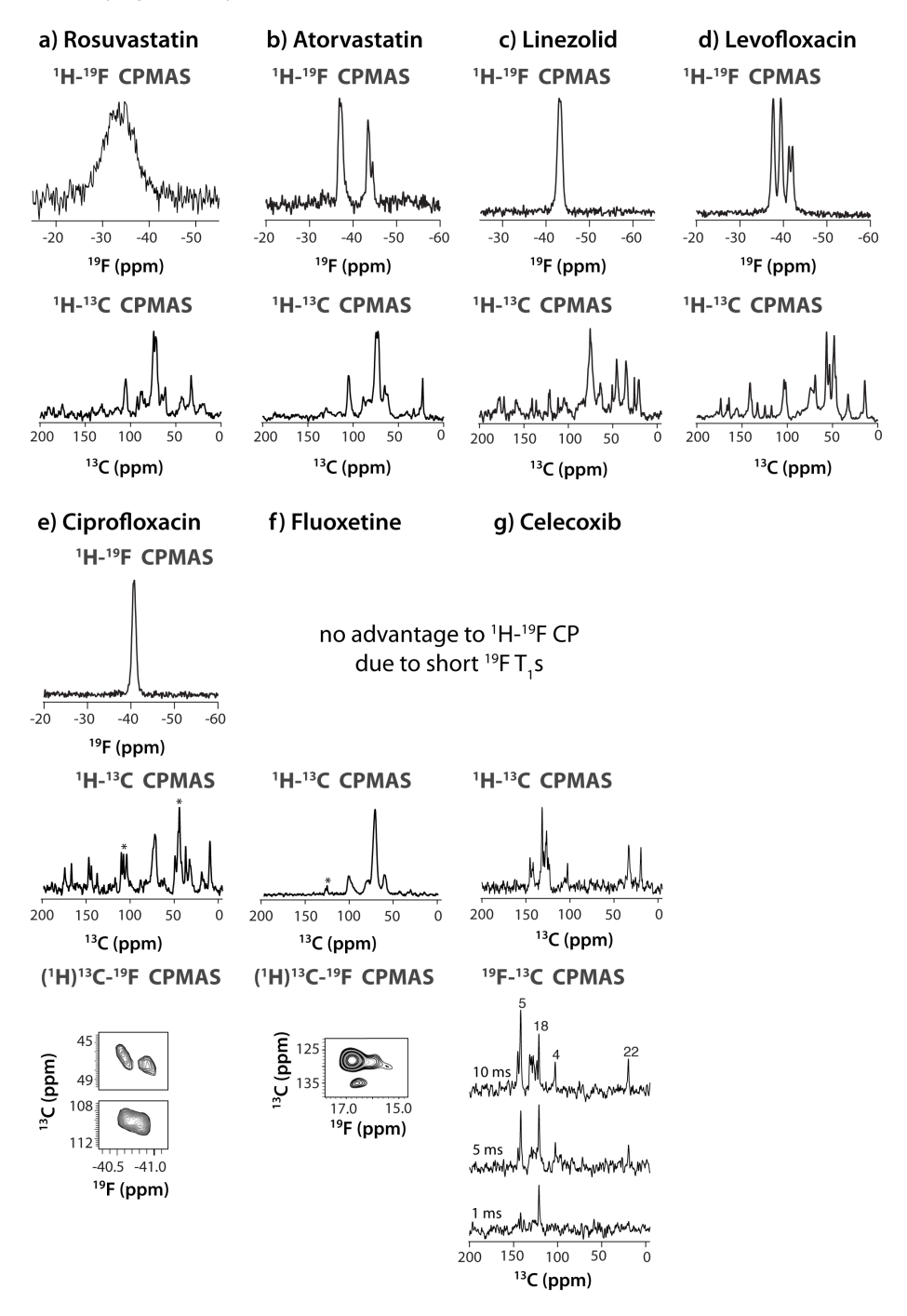


Figure 2. 1D and 2D MAS NMR spectra of of APIs in different drug formulations: a) rosuvastatin, b) atorvastatin, c) linezolid, d) levofloxacin, e) ciprofloxacin, f) fluoxetine, and g) celecoxib. Peaks that appear in the (¹H)-¹³C-¹9F 2D HETCOR spectra of ciprofloxacin and fluoxetine are labeled with asterisks. ¹9F-¹³C CPMAS spectra of celecoxib were acquired with contact times of 1 ms, 5 ms, and 10 ms (shown next to the individual traces). Several unique peaks could be assigned and are labeled with atom numbers (Fig. 1). The MAS frequency was 60 kHz. Other experimental conditions are detailed in the Methods section.

In contrast to the ease and speed with which 1D ¹⁹F NMR spectra were collected, ¹³C-detected ¹H-¹³C or ¹⁹F-¹³C CPMAS experiments (Figure 2b,d) required 3-6 hours of signal averaging to achieve comparable signal-to-noise ratios (SNR). Notably, in formulations with a low percentage of API, the ¹³C signals are dominated by the excipients rather than the API.

 19 F spectral features, such as chemical shifts and line widths, are very sensitive to the chemical structure and the drug formulation. Line widths vary substantially, from 0.4 ppm in fluoxetine (δ_{iso} = 16.8 ppm) to 7.6 ppm in rosuvastatin (peak center at -33.8 ppm). On the basis of the linewidths alone we can conclude that rosuvastatin is amorphous while the other formulations comprise mono- or polycrystalline APIs.

Interestingly, the 19 F 1D and/or 2D spectra suggest the presence of at least two distinct species in all samples, except for celecoxib (for which no 2D spectra were acquired). The multiple 19 F species observed in the spectra may correspond to crystallographically inequivalent fluorine atoms or indicate conformational disorder. For ciprofloxacin, the 1 ppm-wide 19 F peak contains two resonances (δ_{iso} = -40.6 and -40.9 ppm), as evidenced by the 2D (1 H) 13 C- 19 F HETCOR spectrum (Figure 2c). For fluoxetine, the 2D (1 H) 13 C- 19 F HETCOR spectrum reveals that the 19 F peak contains three resonances, a major peak at δ_{iso} = 16.8, and two minor peaks at δ_{iso} = 16.0 and 15.4 ppm. The presence of the two low-intensity resonances suggests some heterogeneity, possibly caused by aging of the API. The 13 C chemical shifts of resonances correlated with each unique fluorine species in fluoxetine and ciprofloxacin are also distinct, as evidenced by the HETCOR spectra. Spectra for atorvastatin and levofloxacin each exhibit at least four individual 19 F signals. The spectrum of linezolid possesses 2 very similar resonances whose chemical shifts differ by only 0.35 ppm.

To evaluate the polarization buildup of ¹⁹F-¹³C magnetization, a series of ¹⁹F-¹³C 1D spectra were acquired on celecoxib (Figure 2d) with CP contact times ranging from 1 ms to 10 ms. At short contact times, ¹³C resonances for atoms within 1-2 bonds of the fluorine atoms appear, while longer-range ¹⁹F-¹³C correlations, corresponding to dipolar transfers between atoms separated by several bonds, emerge at longer mixing times.

Intrigued by the observation of 4 peaks in the ¹⁹F MAS NMR spectrum of levofloxacin (provided in Figure 3a with atoms numbered), we performed a series of 1D and 2D experiments, to elucidate the molecular structure of the API in the two formulations. It is apparent that the four peaks comprise two sets of resonances, at -37.7 and -39.5 ppm (peaks I and II, group A) and -41.4 and -42.1 ppm (peaks III and IV, group B) in both formulations (Figure 3b). Within each group, the two resonances are of equal integrated intensity, suggesting the presence of two polymorphs. Indeed, two ¹⁹F resonances had been reported previously for the hemihydrate of levofloxacin corresponding to two crystallographically inequivalent molecules,⁴⁴ whose chemical shifts were very similar to those of group A resonances observed here (-37.7 and -39.5 ppm). Importantly, the relative intensities of group A and group B resonances differ for the two formulations investigated here (Figure 3b),

suggesting that different ratios of the two polymorphs are present in the formulations by different manufacturers. In the 2D ¹⁹F-¹⁹F RFDR spectra recorded with mixing times of up to 100 ms, cross peaks are observed between each pair of resonances within group A and group B, but no cross peaks between the two groups are seen (Figure 3c, S3), corroborating the hypothesis that group A and group B belong to two different polymorphs.

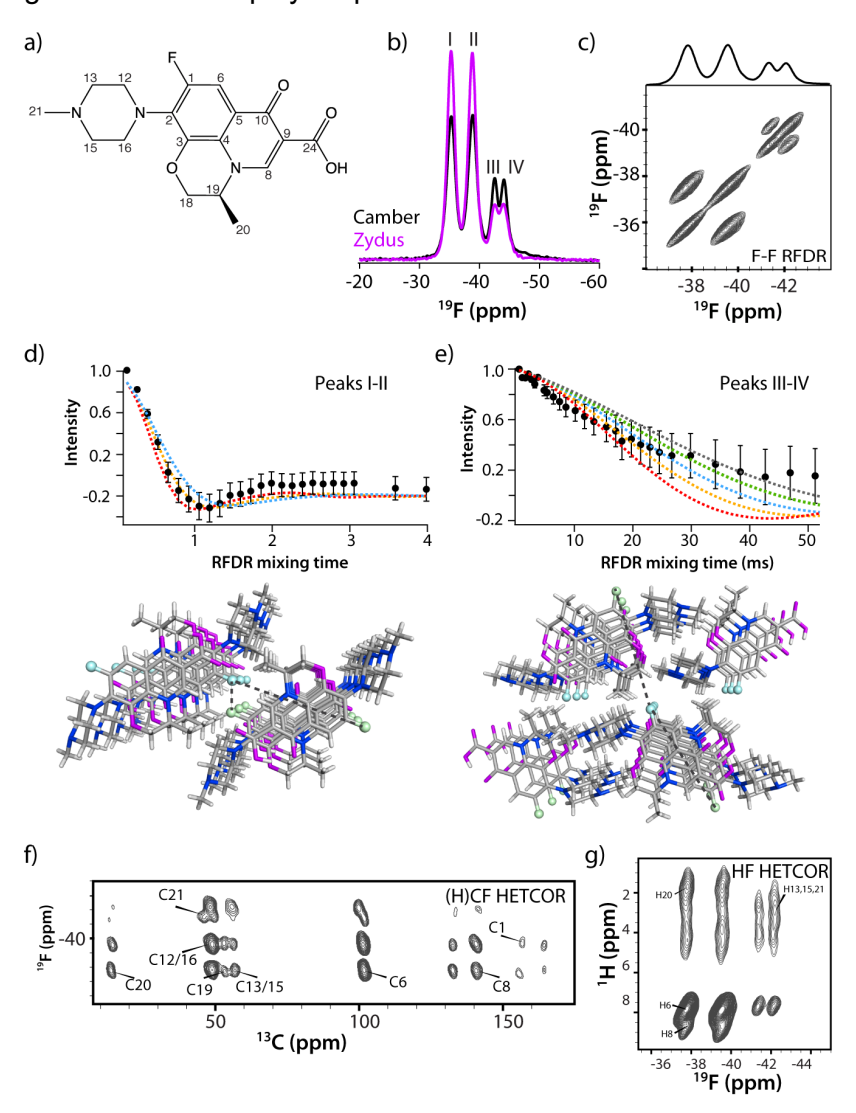


Figure 3. a) Structure of levofloxacin with IUPAC numbering. b) ¹⁹F 1D spectra of levofloxacin formulations from two manufacturers (Camber, black and Zydus, magenta). c) ¹⁹F-¹⁹F RFDR 2D spectrum of levofloxacin (Camber) acquired with the mixing time of 30 ms. d) Experimental (•) and simulated (—) ¹⁹F DANTE-RFDR exchange curves for peak pairs I-II (top) and the X-ray structure of levofloxacin, depicting short-range ¹⁹F-¹⁹F interactions observed in DANTE-RFDR by dashed lines (bottom, CSD-YUJNUM01⁴⁴). Exchange profiles for peaks I-II were simulated using a 2-spin approximation with interfluorine distances of 2.7 Å (red), 2.9 Å (gold), and 3.1 Å (blue). Crystallographically equivalent fluorine atoms are shown in the same color (light blue or green). e) Experimental (•) and simulated (—) ¹⁹F DANTE-RFDR exchange curves for resonance pairs III-IV (top) and the X-ray structure of levofloxacin (P2₁ space group) depicting long-range ¹⁹F-¹⁹F interactions between crystallographically inequivalent fluorine atoms by dashed lines; (bottom, CSD-YUJPAU01⁴⁵). Exchange profiles for peaks III-IV were simulated using a 2-spin approximation with interfluorine distances of 9.5 Å (red), 10 Å (gold), 10.5 Å (blue), 11 Å (green), and 11.5 Å (grey). f,g) (¹H)¹³C-¹⁹F HETCOR and ¹H-¹⁹F HETCOR spectra of levofloxacin (Camber).

To assess the arrangement of the levofloxacin molecules in the crystal lattice, we performed 1D ¹⁹F DANTE-RFDR experiments.¹³ The very rapid exchange observed between the two deshielded resonances I and II suggests a very short, <3 Å interfluorine distance between them (Figure 3d, S5). Indeed, the 2-spin system simulation with an interfluorine distance of 2.9 Å captures the experimental data very well (Figure 3d, solid lines). Deviations between experiment and simulation at longer mixing times are due to multi-spin effects, associated with the contributions from multiple fluorine atoms in the crystal lattice. The short ¹⁹F interflourine distance in this polymorph is consistent with frequently observed crystal structures of levoflaxicin⁴⁵⁻⁴⁷ (Figure 3d). 2D ¹H-¹⁹F and (¹H)¹³C-¹⁹F HETCOR spectra provide further information about the intermolecular interactions present in this polymorph, also consistent with known crystal structures of levofloxacin (Figure S4). Specifically, the following intermolecular ¹H-¹⁹F and ¹³C-¹⁹F interactions were identified: F-H8, F-H20, F-C8, F-C19, and F-C20. The calculated ¹⁹F chemical shifts summarized in Table S1 of the Supporting Information are in good agreement with the experimental data corroborating structure for this polymorph.

The two fluorine species associated with the shielded peaks (resonances III and IV) are suggestive of a very different crystalline environment. The slow DANTE-RFDR magnetization exchange (Figure 3e, S5) indicates a long interfluorine distance and the simulated curve using the 2-spin approximation is generally consistent with an interfluorine distance of 10 Å; the remaining differences between experiment and simulation are due to multi-spin effects, which were not accounted for in simulations. The cross peaks in the 2D (¹H)-¹³C-¹9F and ¹H-¹9F HETCOR spectra (Figure 3f and g, respectively) are also very different for this group of resonances. Several cross peaks are missing or significantly weaker, such as C8/H8 and C19/C20/H20, suggesting a different intermolecular organization in this crystalline polymorph.

Atorvastatin calcium exists in numerous crystalline and amorphous forms. High-resolution structural characterization of this drug has proven to be particularly difficult. For the two generic formulations of atorvastatin, manufactured by Teva (Sample 1) and Apotex (Sample 2), ¹⁹F MAS NMR spectra are markedly different. The spectrum of Sample 1 exhibits a pair of sharp, well-resolved resonances at -40.1 and -41.9 ppm (Figure 4a). In Sample 2, at least four ¹⁹F species can be distinguished, with chemical shifts of -36.9, -37.3, -43.6, and -45.5 ppm. The ¹⁹F T₁s of the individual species are also clearly different between the two samples, with those in Sample 1 being considerably shorter than in Sample 2 (Table S1). Both spectra suggest that the APIs are crystalline, as evidenced by the overall narrow lines compared to amorphous formulations, such as rosuvastatin. The ¹⁹F-¹⁹F 2D RFDR spectrum further supports this notion revealing that each broader peak in sample 2 compared to sample 1 comprises multiple narrow resonances with very similar chemical shifts. These individual resonances correspond to distinct crystalline environments in sample 2. Notably, the ¹⁹F spectrum of Sample 1 is in excellent agreement with the ¹⁹F spectrum reported

previously for pure atorvastatin calcium form I^{48,49} (correcting for TFA vs. CFCl₃ referencing). Sample 2 has similar ¹⁹F chemical shifts to those reported for the form referred to in the literature as "form X".⁴⁹ However, there are notable differences. In Sample 2, the intensity ratio of the two primary resonances (peaks I and II) is 0.75:1, significantly higher than the much lower ratio observed in the pure material. In addition, while in neat form X only two resonances are observed, in the commercial formulation studied here, several additional species are present (a, b, c, d).

To further characterize the atorvastatin samples, 2D ¹H-¹⁹F HETCOR spectra were acquired (Figure 4d). Since these samples contain only 6-9 % w/w API, it is remarkable that high SNR data sets were obtained in a few hours. Such spectra could be indispensable for elucidating the higher order arrangements of the API in the various formulations. The ¹H-¹⁹F HETCOR spectrum of Sample 1 (magenta trace) indicates distinct local environments for each of the two fluorine moieties. Interestingly, some cross peaks are present at ¹H chemical shifts not associated with any Atorvastatin protons (e.g., 5-6 ppm ⁴⁸) and may arise from intermolecular correlations between the API and the excipients.

In the ¹H-¹⁹F HETCOR spectrum of Sample 2 (grey trace), the deshielded group of resonances (collectively labeled I in Figure 4a, centered at -37 ppm) exhibit very different ¹H-¹⁹F correlations compared to those of the shielded group of resonances (collectively labeled II, centered at -44 ppm). Therefore, the deshielded and the shielded resonances are associated with distinct local environments. In contrast, species associated with the same subset of resonances are generally quite similar, although slightly different local environments may be present, as evidenced by the differences in the cross peak patterns. The 2D ¹⁹F-¹⁹F RFDR spectrum of Sample 2 (Figure 4e) reveals additional structural details. While two distinct shielded resonances are present in the 1D ¹⁹F data set, it is clear from the 2D RFDR spectrum that there are at least four unique fluorine atom environments present. At a relatively short mixing time of 20 ms, many cross peaks are observed within the shielded group of resonances, with several of these connecting the shielded and deshielded groups. In the 100 ms mixing time spectrum, additional cross peaks among the various species are present. Such detail would likely not be distinguishable in the fluorine resonances at slower MAS frequencies.

The DANTE-RFDR exchange curves for both formulations (Figure 4b, S6) can be simulated assuming a two-spin system, in which magnetization exchange occurs between two magnetically inequivalent fluorine atoms, separated by at least 12 Å. In atorvastatin calcium crystals, lamellar type packing can be observed, and in these membrane-like structures the bulky hydrophobic moiety comprises the outer layer with the calcium ion coordinated by the hydrophilic groups of the inner layer⁵⁰. Fluorine atoms reside in two distinct electronic environments in the inner layer. In known structures of atorvastatin calcium, the distances between the neighboring fluorine atoms within each type of environment are ~5 Å, while the closest distances between the atoms belonging to two

different environments are ~10-16 Å⁵⁰⁻⁵² (Figure 4c). Since DANTE-RFDR magnetization exchange occurs between peaks with different chemical shifts, groups of resonances labeled I and II in Figure 4a must therefore correspond to fluorine atoms belonging to the different environments separated by ~12 Å. Conversely, fluorine atoms closer to each other (~5 Å apart) must have similar or identical ¹⁹F chemical shifts and do not contribute to the observed DANTE-RFDR exchange curves.

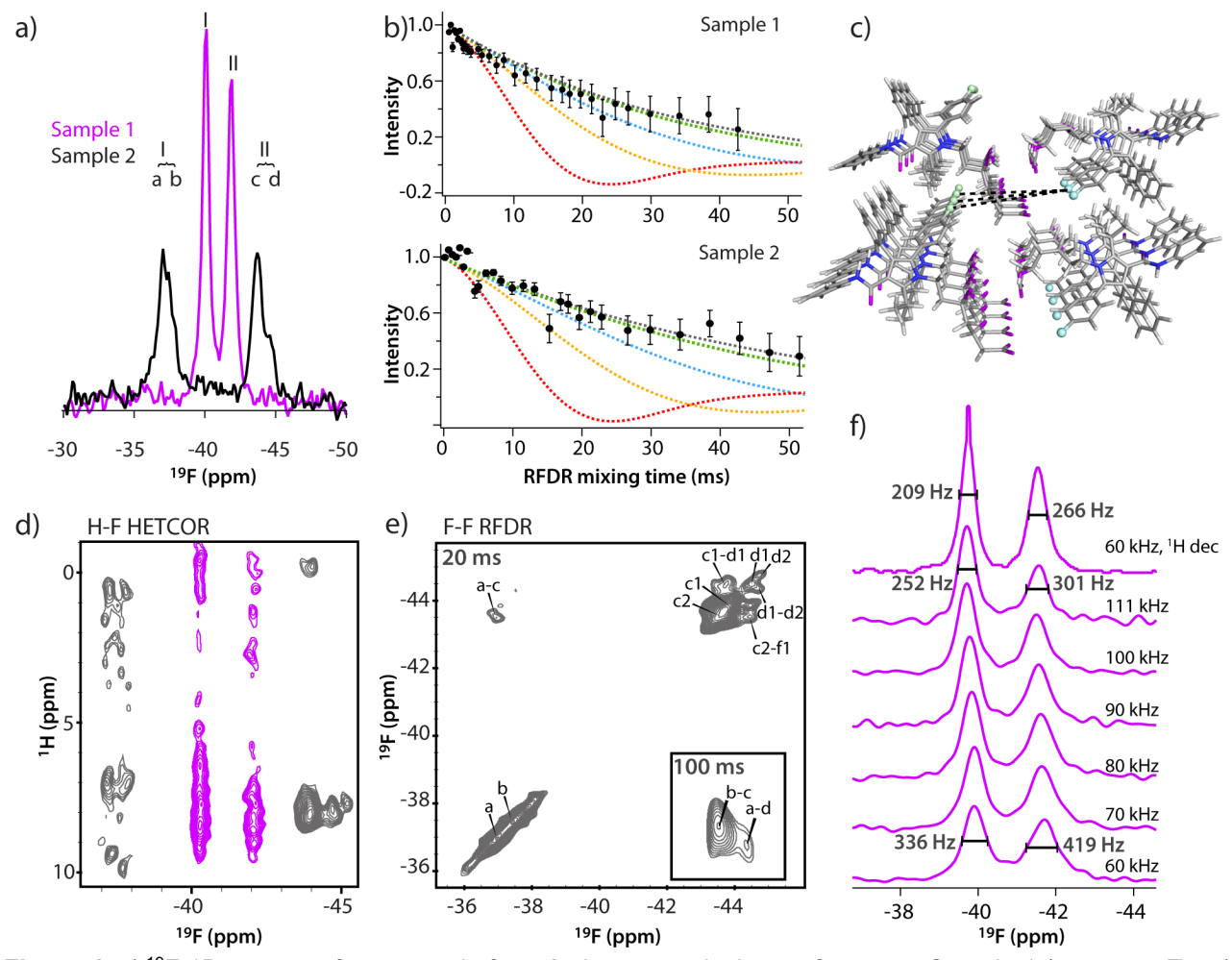


Figure 4. a) ¹⁹F 1D spectra of atorvastatin from 2 pharmaceutical manufacturers: Sample 1 (magenta; Teva), Sample 2 (grey; Apotex). b) Experimental (•) and simulated (—) ¹⁹F DANTE-RFDR exchange curves for Sample 1 (top) and Sample 2 (bottom). Exchange profiles were simulated using a 2-spin approximation with interfluorine distances of 8 Å (red), 10 Å (gold), 12 Å (blue), 15 Å (green), and 17 Å (grey). c) Structure of atorvastatin calcium form I⁵¹. Fluorine atoms are shown as spheres, with crystallographically equivalent fluorines shown in the same color (teal or green). Long-range F-F interactions between non-equivalent fluorine atoms are indicated by dashed lines. Ca²⁺ ions and H₂O molecules are omitted for clarity. d) ¹H-¹⁹F HETCOR spectra of atorvastatin Sample 1 (magenta) and Sample 2 (grey). e) ¹⁹F-¹⁹F RFDR 2D spectrum of atorvastatin (Sample 2) acquired with a 20 ms mixing time; the MAS frequency was 60 kHz. The inset (lower right) shows the cross-peaks in the RFDR spectrum acquired with a 100 ms mixing time; the MAS frequency was 111 kHz. f) ¹⁹F 1D spectra of Sample 1 acquired at MAS frequencies ranging from 60 to 111 kHz (listed next to each spectrum). The top spectrum was acquired with ¹H decoupling, all others were recorded without decoupling.

For sample 2 we also performed a systematic evaluation of the ¹⁹F line width as a function of the MAS frequency and ¹H decoupling. As shown in Figure 4f, ¹H decoupling increases the resolution dramatically: at 60 kHz, the widths of the lines are reduced from 419 to 266 Hz and from 336 to 209

Hz for the shielded and deshielded peak, respectively, upon ¹H decoupling. Increasing the spinning frequency from 60 to 111 kHz, in the absence of ¹H decoupling, also resulted in a significant narrowing of the ¹⁹F resonances, from 419 to 301 and from 336 to 252 Hz for the shielded and deshielded resonances, respectively. Taken together, these results indicate that even at 111 kHz MAS, ¹H-¹⁹F dipolar interactions still contribute significantly to the observed ¹⁹F line widths. Comparing the sensitivity of the 1.3 and 0.7 mm rotors, the signal-to-noise ratios of the spectra acquired at 60 kHz and 111.11 kHz are 21.4 and 21.2 respectively for the peak at -40 ppm, yielding an effective SNR per mg per square root of scan of 1.8 (60 kHz MAS, 3 mg material) and 10.6 (111 kHz, 0.5 mg material). It is important to note the excellent resolution of the 60 kHz spectra with ¹H decoupling, given that probes capable of 110 kHz MAS are not yet widely available.

In contrast to levofloxacin and atorvastatin, the spectra of the amorphous rosuvastatin are similar for all three formulations investigated here (Figure 5a). To order to uncover the origin of the very broad line, we performed ^{19}F DANTE inversion-based experiments 13 . The spectra shown in Figure 5b indicate that the broad peak comprises a continuum of resonances, with δ_{iso} spanning from -26.7 to -40.8 ppm, and homogeneous line widths are of the order of 1 ppm.

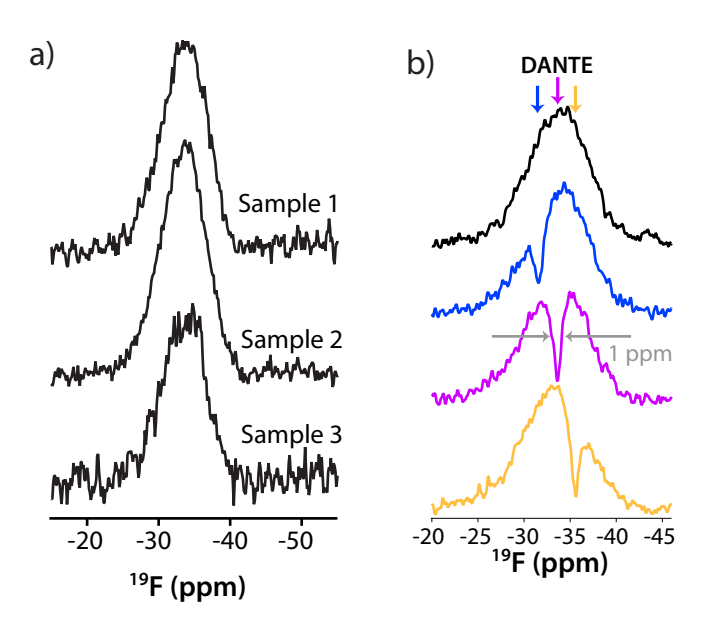


Figure 5. a) ¹⁹F spectra for rosuvastatin calcium generic formulations from three different manufacturers (BioCon, Sample 1; Kanon Pharma, Sample 2; Tris Pharma, Sample 3). b) A series of ¹⁹F DANTE-based spectra for Sample 3. DANTE inversion pulses were applied to the frequencies labeled by arrows. The homogeneous line width is of the order of 1 ppm.

CONCLUSIONS

Taken together, the present results clearly demonstrate that fluorine NMR is uniquely suited to probe pharmaceutical formulations of fluorine-containing drugs. The power of ¹⁹F MAS NMR using sample spinning frequencies in the range of 60-111 kHz lies in its exquisite sensitivity (allowing for very fast data collection, even with very small amounts of material) and specificity (chemical shifts report directly on the API and are sensitive to differences in formulation and/or excipients). We anticipate being able to routinely detect conformational heterogeneity and uncover detailed structural information for fluorinated APIs using selective inversion and correlation experiments. Overall, the approach presented here establishes a framework for structural analysis of fluorinated APIs with fast magic angle spinning and is envisioned to be powerful for the identification and quantification of API polymorphs in pharmaceutical formulations.

ACKNOWLEDGMENTS

This work was supported by the National Science Foundation (NSF Grant CHE-1708773 to AMG and TP) and by the National Institutes of Health (NIH Grant P50AI150481, Technology Development Project 2) and is a contribution from the Pittsburgh Center for HIV Protein Interactions. We acknowledge the support of the National Institutes of Health (NIH Grant P30GM110758) for the support of core instrumentation infrastructure at the University of Delaware.

AUTHOR CONTRIBUTIONS

T.P. and A.M.G. conceived the project and guided the work. C.M.Q., J.O.S, and T.P. performed the NMR experiments and analyzed the data. R.Z. processed the DANTE-RFDR data and performed simulations. T.P., C.M.Q., and A.M.G. took the lead in writing the manuscript. All authors discussed the results and contributed to the manuscript preparation.

SUPPORTING INFORMATION

1D ¹H spectra of all drug formulations; ¹⁹F and ¹H spin-lattice relaxation; slow MAS spectra of atorvastatin and levofloxacin; additional DANTE-RFDR simulations of atorvastatin; MAS frequency and ¹H-decoupling dependence of atorvastatin ¹⁹F spectra; DFT calculations of ¹⁹F isotropic chemical shifts; example DANTE-RFDR SIMPSON simulation script. This information is available online at http://pubs.acs.org.

CONFLICT OF INTEREST

The authors declare no conflict of interest.

REFERENCES

- (1) Inoue, M.; Sumii, Y.; Shibata, N. Contribution of organofluorine compounds to pharmaceuticals. *ACS Omega* **2020**, *5*, 10633-10640.
- (2) Mei, H. B.; Han, J. L.; Fustero, S.; Medio-Simon, M.; Sedgwick, D. M.; Santi, C.; Ruzziconi, R.; Soloshonok, V. A. Fluorine-containing drugs approved by the FDA in 2018. *Chem. Eur. J.* **2019**, 25, 11797-11819.
- (3) Zhou, Y.; Wang, J.; Gu, Z.; Wang, S.; Zhu, W.; Luis Acena, J.; Soloshonok, V. A.; Izawa, K.; Liu, H. Next generation of fluorine-containing pharmaceuticals, compounds currently in phase II-III clinical trials of major pharmaceutical companies: new structural trends and therapeutic areas. *Chem. Rev.* **2016**, *116*, 422-518.
- (4) Mei, H.; Remete, A. M.; Zou, Y.; Moriwaki, H.; Fustero, S.; Kiss, L.; Soloshonok, V. A.; Han, J. Fluorine-containing drugs approved by the FDA in 2019. *Chin. Chem. Lett.* **2020**, *31*, 2401-2413.
- (5) Gillis, E. P.; Eastman, K. J.; Hill, M. D.; Donnelly, D. J.; Meanwell, N. A. Applications of fluorine in medicinal chemistry. *J. Med. Chem.* **2015**, *58*, 8315-8359.
- (6) Hong, Y.-I.; Manjunatha Reddy, G. N.; Nishiyama, Y. Selective detection of active pharmaceutical ingredients in tablet formulations using solid-state NMR spectroscopy. Solid State Nucl. Magn. Reson. 2020, 106, 101651.
- (7) Geppi, M.; Mollica, G.; Borsacchi, S.; Veracini, C. A. Solid-state NMR studies of pharmaceutical systems. *Appl. Spectrosc. Rev.* **2008**, *43*, 202-302.
- (8) Lubach, J. W.; Munson, E. J. Solid-state nuclear magnetic resonance of pharmaceutical formulations. *Encyclopedia of Analytical Chemistry* **2013**, 1-18.
- (9) Pindelska, E.; Sokal, A.; Kolodziejski, W. Pharmaceutical cocrystals, salts and polymorphs: advanced characterization techniques. *Adv. Drug Deliv. Rev.* **2017**, *117*, 111-146.
- (10) Gerig, J. T. Fluorine NMR of proteins. Prog. Nucl. Magn. Reson. Spectrosc. 1994, 26, 293-370.
- (11) Gee, C. T.; Arntson, K. E.; Urick, A. K.; Mishra, N. K.; Hawk, L. M. L.; Wisniewski, A. J.; Pomerantz, W. C. K. Protein-observed ¹⁹F-NMR for fragment screening, affinity quantification and druggability assessment. *Nat. Protoc.* **2016**, *11*, 1414-1427.
- (12) Boeszoermenyi, A.; Chhabra, S.; Dubey, A.; Radeva, D. L.; Burdzhiev, N. T.; Chanev, C. D.; Petrov, O. I.; Gelev, V. M.; Zhang, M.; Anklin, C.; Kovacs, H.; Wagner, G.; Kuprov, I.; Takeuchi, K.; Arthanari, H. Aromatic ¹⁹F-¹³C TROSY: a background-free approach to probe biomolecular structure, function, and dynamics. *Nat. Methods* **2019**, *16*, 333-340.
- (13) Fritz, M.; Kraus, J.; Quinn, C. M.; Yap, G. P. A.; Struppe, J.; Sergeyev, I. V.; Gronenborn, A. M.; Polenova, T. Measurement of accurate interfluorine distances in crystalline organic solids: a high-frequency magic angle spinning NMR approach. *J. Phys. Chem. B* **2019**, *123*, 10680-10690.
- (14) Lu, M. M.; Ishima, R.; Polenova, T.; Gronenborn, A. M. ¹⁹F NMR relaxation studies of fluorosubstituted tryptophans. *J. Biomol. NMR* **2019**, 73, 401-409.
- (15) Lu, M. M.; Polenova, T. E.; Gronenborn, A. M. ¹⁹F NMR studies of cyclophilin A and its interaction with HIV-1 capsid. *Biophys. J.* **2020**, *118*, 503a-503a.
- (16) Lu, M. M.; Sarkar, S.; Wang, M. Z.; Kraus, J.; Fritz, M.; Quinn, C. M.; Bai, S.; Holmes, S. T.; Dybowski, C.; Yap, G. P. A.; Struppe, J.; Sergeyev, I. V.; Maas, W.; Gronenborn, A. M.; Polenova, T. ¹⁹F magic angle spinning NMR spectroscopy and density functional theory calculations of fluorosubstituted tryptophans: integrating experiment and theory for accurate determination of chemical shift tensors. *J. Phys. Chem. B* **2018**, *122*, 6148-6155.
- (17) Lu, M. M.; Wang, M. Z.; Sergeyev, I. V.; Quinn, C. M.; Struppe, J.; Rosay, M.; Maas, W.; Gronenborn, A. M.; Polenova, T. ¹⁹F dynamic nuclear polarization at fast magic angle spinning for NMR of HIV-1 capsid protein assemblies. *J. Am. Chem. Soc.* **2019**, *141*, 5681-5691.
- (18) Matei, E.; André, S.; Glinschert, A.; Infantino, A. S.; Oscarson, S.; Gabius, H. J.; Gronenborn, A. M. Fluorinated carbohydrates as lectin ligands: dissecting glycan-cyanovirin interactions by using ¹⁹F NMR spectroscopy. *Chemistry* **2013**, *19*, 5364-5374.
- (19) Matei, E.; Gronenborn, A. M. ¹⁹F paramagnetic relaxation enhancement: a valuable tool for distance measurements in proteins. *Angew. Chem. Int. Ed.* **2016**, *55*, 150-154.

- (20) Norton, R. S.; Leung, E. W. W.; Chandrashekaran, I. R.; MacRaild, C. A. Applications of ¹⁹F-NMR in fragment-based drug discovery. *Molecules* **2016**, *21*, 860.
- (21) Roos, M.; Mandala, V. S.; Hong, M. Determination of long-range distances by fast magic-angle-spinning radiofrequency-driven ¹⁹F-¹⁹F dipolar recoupling NMR. *J. Phys. Chem. B* **2018**, *122*, 9302-9313.
- (22) Roos, M.; Wang, T.; Shcherbakov, A. A.; Hong, M. Fast magic-angle-spinning ¹⁹F spin exchange NMR for determining nanometer ¹⁹F-¹⁹F distances in proteins and pharmaceutical compounds. *J. Phys. Chem. B* **2018**, *122*, 2900-2911.
- (23) Sharaf, N. G.; Ishima, R.; Gronenborn, A. M. Conformational plasticity of the NNRTI-binding pocket in HIV-1 reverse transcriptase: a fluorine nuclear magnetic resonance study. *Biochemistry* **2016**, *55*, 3864-3873.
- (24) Sharaf, N. G.; Xi, Z.; Ishima, R.; Gronenborn, A. M. The HIV-1 p66 homodimeric RT exhibits different conformations in the binding-competent and -incompetent NNRTI site. *Proteins* **2017**, 85, 2191-2197.
- (25) Shcherbakov, A. A.; Hong, M. Rapid measurement of long-range distances in proteins by multidimensional ¹³C-¹⁹F REDOR NMR under fast magic-angle spinning. *J. Biomol. NMR* **2018**, *71*, 31-43.
- (26) Shcherbakov, A. A.; Roos, M.; Kwon, B.; Hong, M. Two-dimensional ¹⁹F-¹³C correlation NMR for ¹⁹F resonance assignment of fluorinated proteins. *J. Biomol. NMR* **2020**, *74*, 193-204.
- (27) Wang, M.; Lu, M.; Fritz, M. P.; Quinn, C. M.; Byeon, I. J. L.; Byeon, C. H.; Struppe, J.; Maas, W.; Gronenborn, A. M.; Polenova, T. Fast magic-angle spinning ¹⁹F NMR spectroscopy of HIV-1 capsid protein assemblies. *Angew. Chem. Int. Ed.* **2018**, *57*, 16375-16379.
- (28) Dalvit, C.; Vulpetti, A. Ligand-based fluorine NMR screening: principles and applications in drug discovery projects. *J. Med. Chem.* **2019**, *62*, 2218-2244.
- (29) Grage, S. L.; Afonin, S.; Ulrich, A. S. ¹⁹F NMR of biomembranes. *Solid-State NMR* **2020**, 6-1-6-43.
- (30) Sharaf, N. G.; Gronenborn, A. M. ¹⁹F-modified proteins and ¹⁹F-vontaining ligands as tools in solution NMR studies of protein interactions. *Meth. Enzymol.* **2015**, *565*, 67-95.
- (31) Urbanova, M.; Brus, J.; Sedenkova, I.; Policianova, O.; Kobera, L. Characterization of solid polymer dispersions of active pharmaceutical ingredients by ¹⁹F MAS NMR and factor analysis. *Spectrochim. Acta A Mol. Biomol. Spectrosc.* **2013**, *100*, 59-66.
- (32) Okaru, A. O.; Brunner, T. S.; Ackermann, S. M.; Kuballa, T.; Walch, S. G.; Kohl-Himmelseher, M.; Lachenmeier, D. W. Application of ¹⁹F NMR spectroscopy for content determination of fluorinated pharmaceuticals. *J. Anal. Methods Chem.* **2017**, *Article ID* 9206297.
- (33) Mattes, A. O.; Russell, D.; Tishchenko, E.; Liu, Y. Z.; Cichewicz, R. H.; Robinson, S. J. Application of ¹⁹F quantitative NMR to pharmaceutical analysis. *Concepts Magn. Reson. Part A* **2016**, *45A*, e21422.
- (34) Lu, X.; Huang, C.; Li, M.; Skomski, D.; Xu, W.; Yu, L.; Byrn, S. R.; Templeton, A. C.; Su, Y. Molecular mechanism of crystalline-to-amorphous conversion of pharmaceutical solids from ¹⁹F magic angle spinning NMR. *J. Phys. Chem. B* **2020**, *124*, 5271-5283.
- (35) Lu, X.; Skomski, D.; Thompson, K. C.; McNevin, M. J.; Xu, W.; Su, Y. Three-dimensional NMR spectroscopy of fluorinated pharmaceutical solids under ultrafast magic angle spinning. *Anal. Chem.* **2019**, *91*, 6217-6224.
- (36) Hahn, E. L. An accurate nuclear magnetic resonance method for measuring spin-lattice relaxation times. *Phys. Rev.* **1949**, *76*, 145-146.
- (37) Bennett, A. E.; Rienstra, C. M.; Auger, M.; Lakshmi, K. V.; Griffin, R. G. Heteronuclear decoupling in rotating solids. *J. Chem. Phys.* **1995**, *103*, 6951-6958.
- (38) Eichele, K. HBA 1.7.5. Universität Tübingen 2015.
- (39) Bodenhausen, G.; Freeman, R.; Morris, G. A. A simple pulse sequence for selective excitation in Fourier transform NMR. *J. Magn. Reson.* **1976**, 23, 171-175.
- (40) Morris, G. A.; Freeman, R. Selective excitation in Fourier transform nuclear magnetic resonance. *J. Magn.Reson.* **1978**, 29, 433-462.
- (41) Shen, M.; Hu, B.; Lafon, O.; Trébosc, J.; Chen, Q.; Amoureux, J.-P. Broadband finite-pulse radio-frequency-driven recoupling (fp-RFDR) with (XY8)41 super-cycling for homo-nuclear

- correlations in very high magnetic fields at fast and ultra-fast MAS frequencies. *J. Magn. Reson.* **2012**, 223, 107-119.
- (42) Lee, W.; Tonelli, M.; Markley, J. L. NMRFAM-SPARKY: enhanced software for biomolecular NMR spectroscopy. *Bioinformatics* **2015**, *31*, 1325-1327.
- (43) Bak, M.; Rasmussen, J. T.; Nielsen, N. C. SIMPSON: a general simulation program for solid-state NMR spectroscopy. *J. Magn. Reson.* **2000**, *147*, 296-330.
- (44) Gorman, E. M.; Samas, B.; Munson, E. J. Understanding the dehydration of levofloxacin hemihydrate. *J. Pharm. Sci.* **2012**, *101*, 3319-3330.
- (45) Singh, S. S.; Thakur, T. S. New crystalline salt forms of levofloxacin: conformational analysis and attempts towards the crystal structure prediction of the anhydrous form. *CrystEngComm* **2014**, *16*, 4215-4230.
- (46) Freitas, J. T. J.; de Melo, C. C.; Viana, O. M. M. S.; Ferreira, F. F.; Doriguetto, A. C. Crystal structure of levofloxacin anhydrates: a high-temperature powder X-ray diffraction study versus crystal structure prediction. *Cryst. Growth Des.* **2018**, *18*, 3558-3568.
- (47) Wei, N.; Jia, L.; Shang, Z.; Gong, J.; Wu, S.; Wang, J.; Tang, W. Polymorphism of levofloxacin: structure, properties and phase transformation. *CrystEngComm* **2019**, *21*, 6196-6207.
- (48) Wang, W. D.; Gao, X.; Strohmeier, M.; Wang, W.; Bai, S.; Dybowski, C. Solid-state NMR studies of form I of atorvastatin calcium. *J. Phys. Chem. B* **2012**, *116*, 3641-3649.
- (49) Brus, J.; Urbanova, M.; Sedenkova, I.; Brusova, H. New perspectives of ¹⁹F MAS NMR in the characterization of amorphous forms of atorvastatin in dosage formulations. *Int. J. Pharm.* **2011**, *409*, 62-74.
- (50) Adhikari, B. R.; Kim, D.; Bae, J. H.; Yeon, J.; Roshan, K. C.; Kang, S. K.; Lee, E. H. New category for active pharmaceutical ingredients, a low molecular weight organogelator: crystal structure of atorvastatin calcium and its unusual phase transition behavior during dissolution. *Cryst. Growth Des.* 2016, 16, 7198-7204.
- (51) Hodge, R. L.; Kaduk, J. A.; Gindhart, A. M.; Blanton, T. N. Crystal structure of atorvastatin calcium trihydrate Form I (Lipitor®), (C33H34FN2O5)2Ca(H2O)3. *Powder Diffr.* 2020, 35, 136-143.
- (52) Gates-Rector, S.; Blanton, T. The powder diffraction file: a quality materials characterization database. *Powder Diffr.* **2019**, *34*, 352-360.

Table of contents graphic

